HANNA BELGHIT*,***, HICHEM FARH*, TOUFIK ZIAR*#, MOSBAH ZIDANI**, MERYEM GUEMINI***

## STUDY OF MECHANICAL PROPERTIES AND PRECIPITATION REACTIONS
## IN LOW COPPER CONTAINING Al-Mg-Si ALLOY

The scope of this work is to investigate the precipitation of two Al-Mg-Si alloys with and without Cu and excess Si by using the differential scanning calorimetry (DSC), transmission electron microscopic (TEM), Vickers hardness measurement and X-ray diffraction. The analysis of the DSC curves found that the excess Si accelerate the precipitation and the alloy contain the excess Si and small addition of copper has higher aging-hardness than that of free alloy (without excess Si and Cu) at the same heat treatment condition. The sufficient holding time for the precipitation of the $\beta''$ phase was estimated to be 6 hours for the alloy aged at 100°C and 10 hours for the alloy aged at 180°C. The low Copper containing Al-Mg-Si alloy gives rise to the forming a finer distribution of $\beta$ (Mg$_2$Si) precipitates which increases the hardness of the alloy. In order to know more about the precipitation reactions, concern the peaks on the DSC curve transmission electron microscopy observation were made on samples annealed at temperatures (250°C, 290°C and 400°C) just above the corresponding peaks of the three phases $\beta''$, $\beta'$ and $\beta$ respectively.

*Keywords*: Al-Mg-Si alloys, precipitation, DSC, TEM, excess Si, Copper

## 1. Introduction

Al-Mg-Si aluminum alloys have been the topic of several scientific research works. The excellent mechanical and electrical properties of these alloys allowed their use in many sectors such as aerospace, automotive and transport of electricity [1-5]. The heat treatable Al-Mg-Si alloys are often selected for this application, because they show up a well combination of weldability, formability and corrosion [6]. The strengthening of the above alloys is based on a precipitation hardening process. The precipitation sequence in these alloys is generally accepted [7-13] to be:

$$(SSS) \rightarrow (G.P) \text{ zones} \rightarrow \beta'' \rightarrow \beta' \rightarrow \beta$$
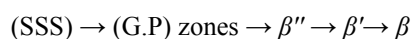
where:
- SSS is the supersaturated solid solution.
- G.P is Guinier and Preston zones
- $\beta''$ is the coherent strengthening phase, which is in the form of needles coherent precipitate growing along a <100> direction of the Al matrix [14]. The structure of $\beta''$ phase was identified as monoclinic with lattice constants of $a = 0.77$ nm, $b = 0.67$ nm and $c = 0.405$ nm [15,16].
- $\beta'$ is the semi-coherent phase, which is in the form of rods growing along a <100> directions of the Al matrix. This phase has hexagonal structure with $a = 0.705$ nm and $c = 0.405$ nm [17,18]

- $\beta$ is the equilibrium phase, which is in the form of small plates with thicknesses of about ten nm and a few hundred nm of size. This phase has a face-centered cubic (FCC) CaF2 structure with $a = 0.639$ nm [19]

The 6xxx series aluminum alloys have low addition elements and are easy to form into extrusions such as: forgings and other shaped products and then to obtain their highest mechanical properties during heat treatment and ageing [20-22].

In the Al-Mg-Si aluminum alloys with Cu and excess Si, the initial heat treatment (T6) condition consists of the usual needle-shaped ternary metastable precipitates in high number density and volume fraction, together with a smaller number and volume fraction of L-phase. L-phase is a coherent precipitates growing along <100> of aluminum matrix, which has a disordered rod or lath morphology. This phase is different from $Q'$ and occurs as a precursor to $Q'$. The majority needles have Cu-free bulks and Cu-enriched interfaces [23]. The Addition of Cu to Al-Mg-Si alloys slows down the formation of solute clusters in an early stage and promotes their subsequent growth in a later stage [24]. The highest Cu addition increases hardness of alloys with higher number densities of shorter precipitates, and reduces the width of precipitate free zones (PFZ's) [25].

The purpose of this research is to investigate the effect of small addition of copper (Cu) on the kinetics transformation and the precipitation in two Al-Mg-Si base and Al-Mg-Excess-Si-Cu alloys.

* UNIVERSITY OF TÉBESSA, FACULTY OF EXACT SCIENCES, DEPARTMENT OF MATERIAL SCIENCES, 12002, ALGERIA
** UNIVERSITÉ DE BISKRA, LABORATOIRE DE GÉNIE ENERGÉTIQUE ET MATÉRIAUX (LGEM), B.P: 145 BISKRA, 07000 ALGÉRIE
*** UNIVERSITY OF OUM EL BOUAGHI, FACULTY OF EXACT SCIENCES, DEPARTMENT OF MATERIAL SCIENCES, BOUAGHI 04000, ALGERIA

# corresponding author: toufik1_ziar@yahoo.fr

## 2. Materials and methods

The composition of the studied alloys is given in Table 1. The alloys were cast, homogenized, hot and cold rolled to 1.9 mm sheets. The sheet samples were solution treated for 15 min at 530°C and then water quenched to room temperature.

The DSC analysis were carried in a SETARAM DSC92 at a heating rate of 5°C/min and the evolution of the microstructure as a function of heat treatments was performed in EM400T analytical electron microscope.

Thin foils for TEM were prepared by spark machining to form discs 3 mm in diameter. The discs were subsequently grounded with fine silicon-carbide emery paper to about 200 mm thick. Final thinning was by jet polishing using a Struers Tenupol Unit with a solution of 33% HNO3 in Analar grade methanol at –10 to –15 volts and a temperature of –20 to –30°C. When the electropolishing was completed the specimens were removed from the solution as quickly as possible and washed with Analar methanol. The specimens were dried between filter papers and then stored in a specimen grid box under vacuum.

Hardness measurements were performed using Vickers hardness tester. The test samples used for hardness measurements were 1×1 cm in size. Hardness data were determined using 10 Kg load. Each measure of Vicker's hardness represents the mean value of at least 10 indentations

TABLE 1

Chemical compositions of the alloys

| Alloys | Mg | Si | Cu | Fe | Mn | Excess Si |
|--------|------|------|-------|------|-------|-----------|
| Alloys 01 | 0,20 | 0,20 | **0,001** | 0,18 | 0,032 | **0,08** |
| Alloys 02 | 0,21 | 0,62 | **0,10** | 0,17 | 0,030 | **0,50** |

## 3. Results and discussion

Fig. 1 shows typical DSC curve obtained at a heating rate of 5°C/min for the alloy 1 immediately after solutionizing and quenching to room temperature. The DSC curves show six main processes marked by (I) to (VI). Out of these processes, three are exothermic reactions tagged as I, III and V and the others processes are endothermic tagged as II, IV and VI. The three exothermic peaks were centered around 106°C (peak I), 270°C (peak III) and 430°C (peak V), respectively. The endothermic peaks (II), (IV) and (VI) appeared at about 224°C, 343°C and 485°C respectively.

The exothermic reaction I corresponding to the early stage clustering of Si-Mg atoms clusters and the formation of G.P zones. This confirms the result that obtained by [26] which revealed the existence of these G.P zones Around 100°C. The exothermic peak III corresponds to the strengthening precipitates $\beta''$ and $\beta'$.

The obtained result is in good agreement with that obtained by [19] which confirms the existence of the $\beta''$ phase at 285°C in the Al–1.12 wt.% Mg₂Si–0.35 wt.% Si alloy. The last exothermic peak V corresponds to the $\beta$ (Mg₂Si) and Si atoms [19,27,28].

Finally, the endothermic peaks (II), (IV) and (VI) appear at temperatures of 224°C, 343°C and 485°C respectively, corresponding to the dissolution of the GP zones and dissolution of the two phases $\beta'$ and ( $\beta$ and / or Si atoms)
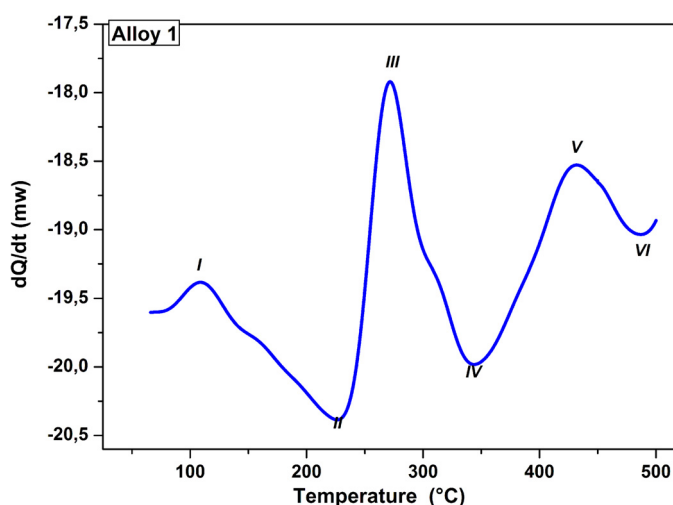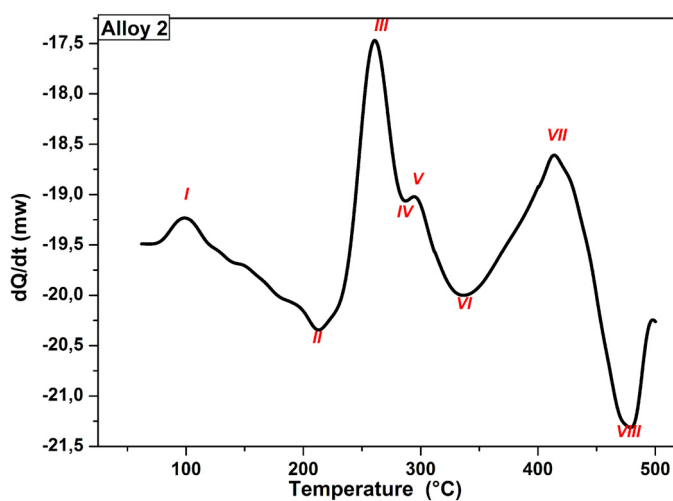


Fig. 1. DSC scan at a heating rate of 05°C/min for alloy 1

Fig. 2 shows the DSC curve of the alloy 2 immediately after solutionizing and quenching to room temperature. Four exothermic reactions tagged as I, III, V and VII and four endothermic labeled as II, IV, VI and VIII were observed.

The exothermic reaction (peak I), appeared at 100°C corresponds to the formation of the GP zones.

The exothermic reaction (peak III), centered near 260°C correspond to the strengthening precipitate $\beta''$ which is formed before the peak-aged condition.

The exothermic reaction (peak V), centered near 294°C is associated with the precipitation of the phase ($\beta'$) and / or phase $Q'$.



Fig. 2. DSC scan at a heating rate of 05°C/min for alloy 2The last exothermic (peak VII), centered near 414°C is attributed to the formation of the equilibrium phase $\beta$.

The endothermic peaks II, IV, VI and VIII appear at temperatures of 212°C, 288°C, 336°C and 477°C respectively,

representing the dissolution of the GP zones and the dissolution of the phases $\beta''$, ($\beta'$ and / or $Q'$) and $\beta$ respectively.

The comparison of the exothermic peaks of the alloy 2 containing the excess Si and a small addition of copper with respect to the exothermic peaks observed in the case of the alloys 1 without excess Si and Cu shows that they are shifted to the low temperatures. It can also be noted that the peak corresponds to the formation of the two phases $\beta''$ and $\beta'$ in the case of the alloy 1 has become two peaks each of which corresponds to the formation of each phase in the case of the alloy 2, Fig. 3. These observations can be related to the excess of silicon contained in the alloy 2. In fact the silicon accelerates the precipitation.
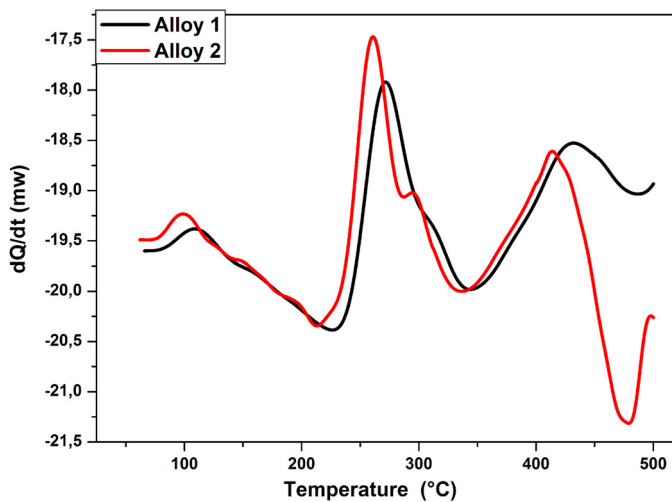


Fig. 3. Superposition of the DSC curves of the two alloys

In order to know more about the precipitation reactions, concern the peaks on the DSC curve of Fig. 2, transmission electron microscopy observation were made on samples annealed at temperatures (250°C, 290°C and 400°C) just above the corresponding peaks of the three phases $\beta''$, $\beta'$ and $\beta$ respectively. The TEM images are obtained with the incident electron beam in the <100> matrix direction.

For the sample heated just above the DSC peak III, Fig. 4. A first sight, some needle-shaped precipitate growing along a [100] direction of the aluminum matrix were observed, this results confirm that the DSC peak III correspond to the strengthening precipitate $\beta''$.

Fig. 5 shows the microstructure of a sample heated just above the DSC peak V. A certain rod-shaped precipitates with different diameters were observed along a [100] direction of the aluminum matrix. The rod-shaped was due to the precipitation of $\beta'$ phase

The microstructure of a sample treated to 400°C (peak VII) was also examined. Large particles with different morphologies and a few large rods were observed, Fig. 6. This observation suggests that the DSC peak IV corresponds to the precipitation of the equilibrium $\beta$ phase.

Fig. 7 shows the variation of microhardness as a function of the aging temperature for the two alloys. It is clear that the alloy 2 containing the excess Si and a small addition of copper
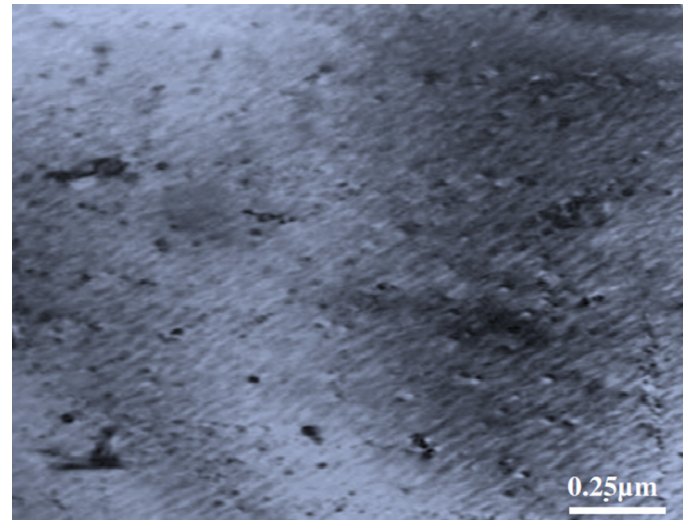


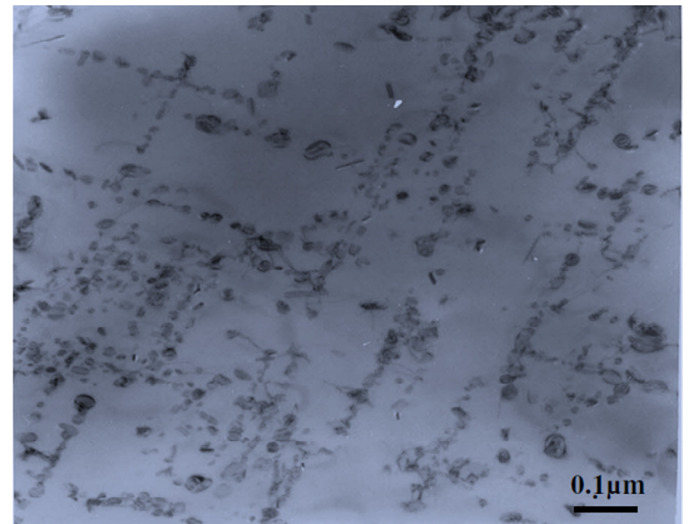Fig. 4. TEM micrograph of the alloy 02 showing the presence of the $\beta''$ phase



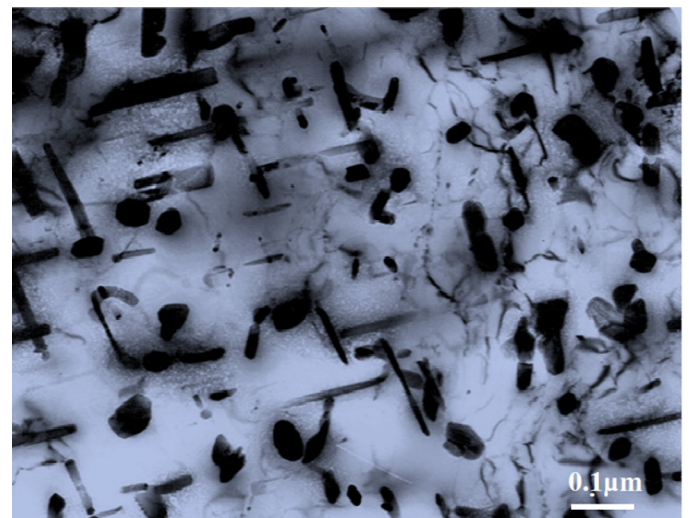Fig. 5. TEM micrograph of the alloy 02 showing the presence of the $\beta'$ phase



Fig. 6. TEM micrograph of the alloy 02 showing the presence of the $\beta$ phase

has hardness higher than that of the alloy 1. This increase in hardness is ascribed to the effect of grain refinement caused by the copper as a result of forming a finer and smaller distribution of $Mg_2Si$ precipitates in higher number but their volume fraction is decreased. This result is in good agreement with the results obtained by Gaber et al. [19]. A shift to a low temperature of the peak corresponds to the strengthening precipitate $\beta''$ in the case of the alloy 02, with respect to that obtained in the alloy 01, is also observed. This observation may be related to the excess silicon contained in the alloy 02, and in that the silicon accelerates the precipitation.

Four peaks were centered at about (75°C, 100°C) for peak I, (250°C, 275°C) for peak II, (325°) for peak III and (425°C) for peak IV are also observed. The first peak is due to the formation of the GP zones, the second peak is associated with the formation of the hardening phase $\beta''$, the third peak is associated with the precipitation of the phase $\beta'$ and the last peak corresponds to the equilibrium phase $\beta$.



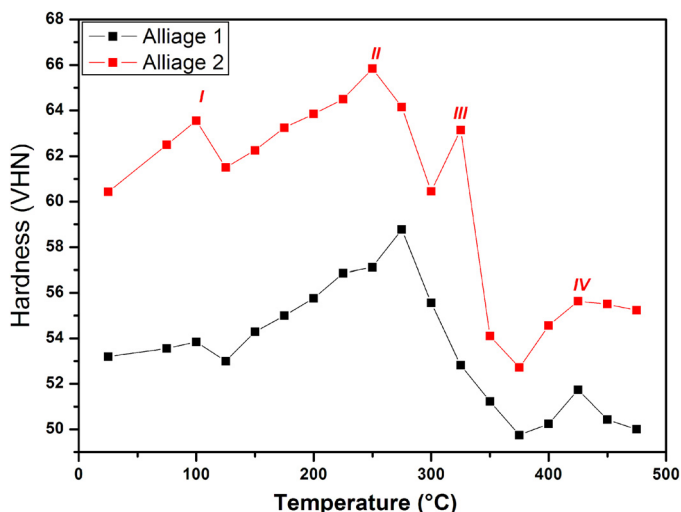Fig. 8. Variation of microhardness as a function of artificial aging time at 100°C



Fig. 7. Variation of microhardness as a function of aging temperature



Fig. 9. Variation of microhardness as a function of artificial aging time at 180°C

Fig. 8 shows the variation of microhardness as a function of the artificial aging time at 100°C for the two alloys. We observe that the microhardness of the two alloys increases with increasing of aging time to a maximum value obtained after 6 hours of holding time.

This is probably due to the formation of clusters of Si and / or Mg. We also note that the increase in hardness in the case of the alloy 2 (contain the excess Si and small addition of copper) is relatively rapid compared to that of the alloy 1 (without excess Si and Cu). This is due to the effect of copper on the precipitation kinetics. The addition of Cu to the alloy increases the number of precipitates and refines the average grain size.

Fig. 9 shows the microhardness curves of the two alloys as a function of the artificial aging time at 180°C. We observe that the microhardness increases with the increasing of the artificial aging t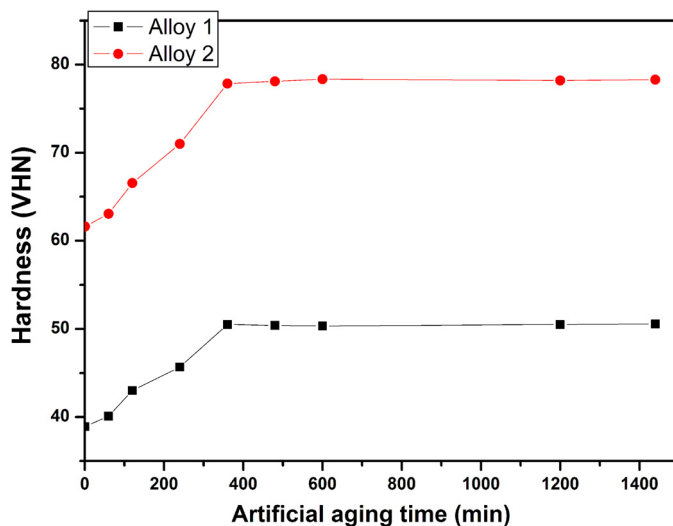ime until reaching a high value after 10 hours of holding time. This time is necessary to initiate the precipitation of the $\beta''$ phase at this temperature. This is in good agreement with the results of [11].
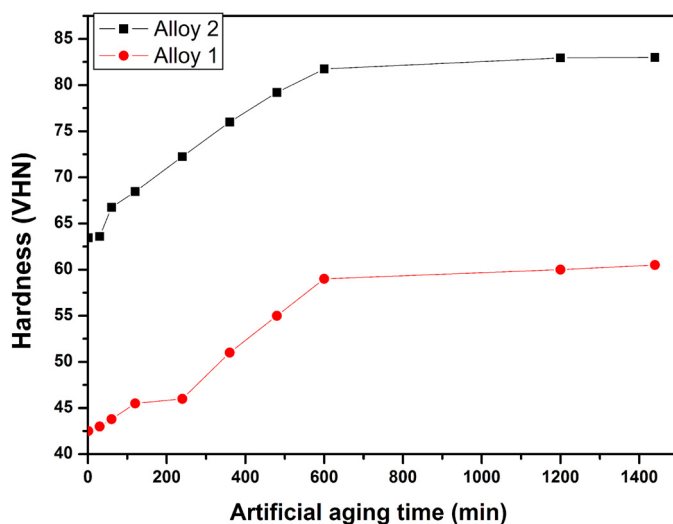
XRD patterns of the two alloys in the initial state (as received) are shown in Fig. 10. The peaks correspond to the C.F.C structure of the $\alpha$-aluminum matrix. The most intense peak is the peak (111) of pure aluminum from the ASTM files.

The same peaks are also observed in the case of the tow alloys homogenized at 550°C for 1 hour, Fig. 11. However, the appearance of certain rays of low intensities means that there is a variation of the lattice parameter of the mesh of the $\alpha$-aluminum matrix due to the presence of the additions elements. The presence of these rays shows the precipitation of the phases in the studied alloys. Table 2 shows the peaks resulting from the addition elements.
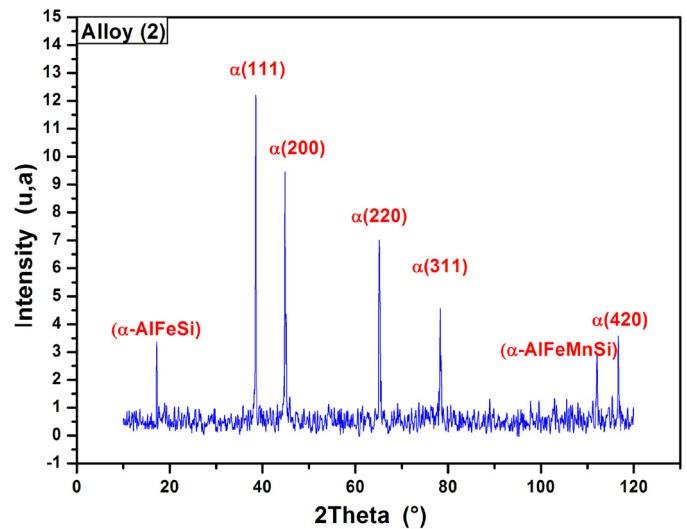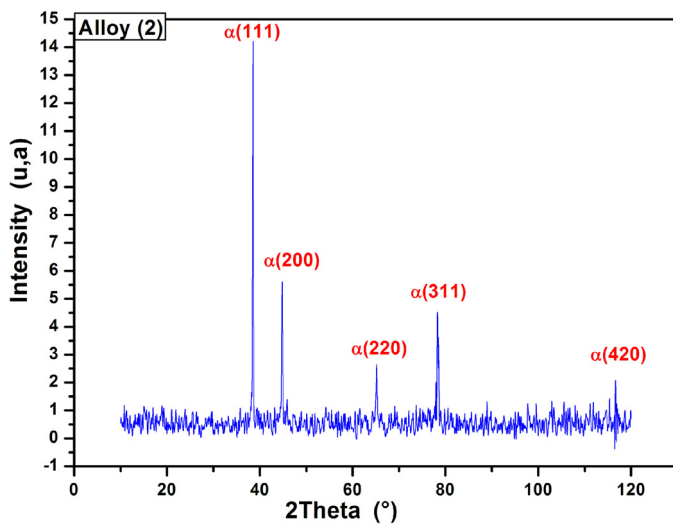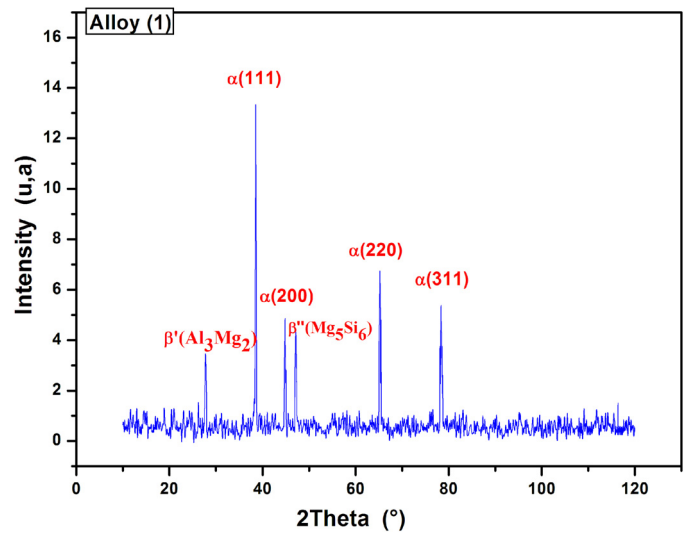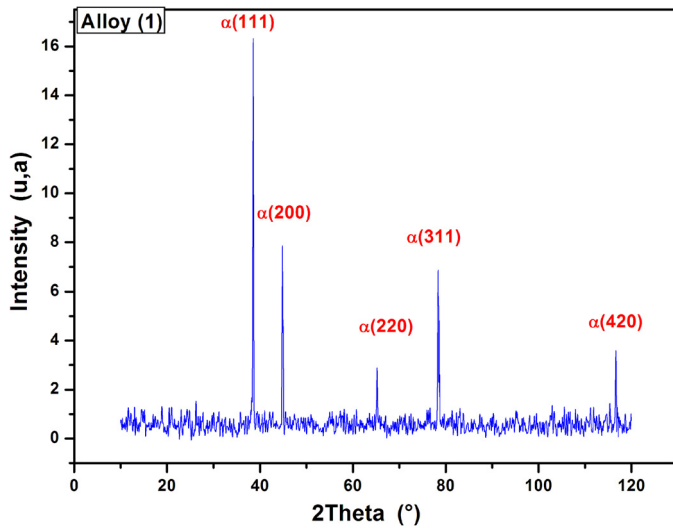
Fig. 10. X-ray diffraction patterns of two alloys in the initial state (as received)



Fig. 11. X-ray diffraction spectrums of two alloys homogenized at 550°C during1 hour and quenched in ice water

TABLE 2

Illustration of the peaks resulting from the additional elements

| $2\theta$ | Phases | References |
|-----------|--------|------------|
| 17.20 | $\alpha$-AlFeSi | [29] |
| 27.76 | $\beta'(Al_3Mg_2)$ | [30,31] |
| 47.16 | $\beta''(Mg_5Si_6)$ | [30,31] |
| 112.06 | $\alpha$-AlFeMnSi | [29,31] |

## 4. Conclusions

The precipitation behavior of Al-Mg-Si alloys with and without Cu and excess Si has been investigated. The use of the differential scanning calorimetry (DSC), transmission electronic microscopy (TEM), X-ray diffraction and Hardness Vickers (Hv) allowed us to define the influence of the addition elements on the precipitation kinetics, and to characterize age-hardening behavior of the Al-Mg-Si alloys.

The precipitation sequence of the two Al-Mg-Si alloys depends on the concentration of the addition elements silicon and low copper. It is obtained that:

• The formation of Guinier and Preston (G.P) zones → the precipitation of the $\beta''$ phase → the precipitation of the $\beta'$ phase → the precipitation of the $\beta$ phase and/or the Si particles.

The low Copper containing Al-Mg-Si alloy gives rise to the forming a finer distribution of $Mg_2Si$ precipitates which increases the hardness of the alloy.

The excess of silicon accelerate the precipitation.

• The sufficient holding time for the precipitation of the $\beta''$ phase was estimated to be 6 hours for the alloy aged at 100°C and 10 hours for the alloy aged at 180°C.

• The homogenization treatment releases a portion of the addition elements responsible for the formation of the precipitates.

1648

## REFERENCES

[1] K. Li, M. Song, Y. Du, X. Fang, Arch. Metal. Mater. **57** (2) (2012).

[2] F. Serradj, R. Guemini, H. Farh, K. Djemmal, Ann. Chim.-Sci. Mat. **35** (1), 59-69 (2010).

[3] M. Zidani, L. Bessais, H. Farh, M. D. Hadid, S. Messaoudi, D. Miroud, M.K. Loudjani, A.L. Helbert, T. Baudin, Steel Compos. Struct. **22** (4), 745-752 (2016).

[4] B. Smyrak, M. Gniełczyk, B. Jurkiewicz, T. Knych, K. Korzeń, M. Jabłoński, A. Mamala, A. Nowak, Key Eng. Mater. **682**, 138-142 (2016).

[5] L. Kucharikova, E. Tillová, M. Matvija, J. Belan, M. Chalupová, Arch. Metal. Mater. **62** (1), 407-415 (2017).

[6] W. Miao, D. Laughlin, Scripta Mater. **40** (7), 873-878 (1999).

[7] G.A. Edwards, K. Stiller, G.L. Dunlop, M.J. Couper, Acta Mater. **46** (11), 3893-3904 (1998).

[8] Y. Aouabdia, A. Boubertakh, S. Hamamda, Mater. Lett. **64** (3), 353-356 (2010).

[9] Y. Birol, Therm Anal Calorim. **83** (1), 219-222 (2006).

[10] W.F. Miao, D.E. Laughlin, Metall. Mater. Trans. A. **31** (2), 361-371 (2000).

[11] M. Murayama, K. Hono, W.F. Miao, D.E. Laughlin, Metall. Mater. Trans. A. **32** (2), 239-246 (2001).

[12] H. Hatta, S. Matsuda, H. Tanaka, H. Yoshida, Inst. Mater. Engi. Australasia, Materials Forum **28**, 564-569 (2004).

[13] T. Ziar, H. Farh, R. Guemini, Acta Metall. Slovaca **22** (3), 138 (2016).

[14] S.J. Andersen, H.W. Zandbergen, J. Jansen, C. Taeholt, U. Tundal, O. Reiso, Acta Mater. **46** (9), 3283-3298 (1998).

[15] K. Matsuda, T. Naoi, K. Fujii, Y. Uetani, T. Sato, A. Kamio, S. Ikeno, Mat. Sci. Eng. A-Struct. **262** (1-2), 232-237 (1999).

[16] S.J. Andersen, C.D. Marioara, M. Torseater, R. Bjorge, F.J.H. Ehlers, R. Holmestad, J. Royset, In Proceedings of the 12th International Conference on Aluminium Alloys, Yokohama, Japan (p. 413-419), (2010).

[17] M.H. Jacobs, Philos. Mag. **26** (1),1-13 (1972).

[18] J.P. Lynch, L.M. Brown, M.H. Jacobs, Acta Metall. **30** (7), 1389-1395 (1982).

[19] A. Gaber, M.A. Gaffar, M.S. Mostafa, E.F.A. Zeid, J. of Alloy Compd. **429** (1-2), 167-175 (2007).

[20] R. Guemini, A. Boubertakh, G.-W. Lorimer, J. Alloy Compd. **486** (1-2), 451-457 (2009).

[21] M. Glogovský, M. Fujda, M. Vojtko, P. Zubko, M. Škrobian, Acta Metall. Slovaca **21** (1), (2015).

[22] Y.X. Lai, B.C. Jiang, C.H. Liu, Z.K. Chen, C.L. Wu, J.H. Chen, J. Alloy Compd. **701**, 94-98 (2017).

[23] C.D. Marioara, S.J. Andersen, J. Røyset, O. Reiso, S. Gulbrandsen-Dahl, T.-E. Nicolaisen, I.-E. Opheim, J.F. Helgaker, R. Holmestad, Metall. Mater. Trans. A. **45** (7), 2938-2949 (2014).

[24] M. Liu, J. Banhart, Mat. Sci. Eng. A-Struct. **658**, 238-245 (2016).

[25] T. Saito, C.D. Marioara, J. Røyset, K. Marthinsen, R. Holmestad, Mat. Sci. Eng. A-Struct. **609**, 72-79 (2014).

[26] K. Djemmal, H. Farh, R. Guemini, M. Zidani, F. Serradj, Int. J. Eng. RS Africa. **28**, 1-7 (2017).

[27] K. Fukui, M. Takeda, T. Endo, Matter. Lett. **59** (11), 1444-1448 (2005).

[28] C. Marioara, S. Andersen, J. Jansen, H. Zandbergen, Acta Mater. **51** (3), 789-796 (2003).

[29] T. Abid, Etude et Caractérisation des Tôles en Alliages Al-Mg-Si. Doctoral thesis, Constantine University 1, Algeria. (2014).

[30] K. Djabri, Etude de l'influence des traitement thermique sur les propriétés des alliages Al-Mg-Si contenants différentes teneurs des éléments d'additions. Master thesis, Tébessa University, Algeria. (2016).

[31] T. Minoda, M. Asano, H. Yoshida, Mate. Sci. Forum. **519-521**, 859-864 (2006).